IEEE Access
Multidisciplinary ⋮ Rapid Review ⋮ Open Access Journal

Received 9 December 2022, accepted 29 December 2022, date of publication 4 January 2023, date of current version 9 January 2023.

*Digital Object Identifier 10.1109/ACCESS.2023.3234118*

RESEARCH ARTICLE

# Multiuser Massive MIMO-OFDM for Visible Light Communication Systems

**MOHAMMAD JAVAD ZAKAVI[1], S. ALIREZA NEZAMALHOSSEINI[1], AND LAWRENCE R. CHEN[2], (Senior Member, IEEE)**

[1]School of Electrical Engineering, Iran University of Science and Technology (IUST), Tehran 1684613114, Iran
[2]Department of Electrical and Computer Engineering, McGill University, Montreal, H3A 0G4, Canada

Corresponding author: S. Alireza Nezamalhosseini (nezam@iust.ac.ir)

This work was supported in part by the Natural Sciences and Engineering Research Council of Canada.

**ABSTRACT** Visible light communication (VLC) has emerged as a viable supplement to existing radio frequency (RF) communication systems. The limited modulation bandwidth of sources is one of the significant challenges in the multiuser (MU) VLC systems, which prohibits transmission at high data rates for each user. Since an array of LEDs is used to illuminate a room, a MU VLC system utilizing massive multiple-input multiple-output (mMIMO) orthogonal frequency-division multiplexing (OFDM) is proposed for achieving high data rates in this paper. Since the distances of the multiple transmitter-receiver links are different, their temporal delays are also different, resulting in complex channel gain and phase differences when transformed to the frequency domain in the OFDM technique. Complex channel vectors associated with different users are mutually spatially orthogonal as the number of transmitters increases. Therefore, inter-user interference (IUI) can be eliminated with simple linear signal processing, and more users can simultaneously communicate in the same time-frequency resource. In this paper, three linear precoding methods, including the maximum ratio transmission (MRT), the minimum mean square error (MMSE), and the zero-forcing (ZF), are investigated for VLC systems based on proposed MU-mMIMO-OFDM in intensity-modulation and direct-detection link. We evaluate and compare the performance of the aforementioned precoding methods in terms of the achievable spectral efficiency and total downlink optical power for different scenarios. Moreover, we derive a closed-form expression for the lower bound on the average achievable sum-rate, which we confirm the accuracy of the derived expression with the numerical simulation. The results demonstrate that the performance of the proposed method in this paper for all precoder techniques, i.e., ZF, MMSE, and MRT, is better than the previous works since the complex channel in the frequency domain is used in this paper. Furthermore, the ZF and MMSE methods are better than MRT when the ratio of the number of LEDs to the number of users is large. At the same time, when this ratio is relatively small, the MRT precoding technique outperforms the ZF and MMSE techniques.

**INDEX TERMS** Visible light communication (VLC), multiuser massive multiple-input multiple-output (MU-mMIMO), orthogonal frequency-division multiplexing (OFDM), precoding.

## I. INTRODUCTION

Visible light communication (VLC) has received much interest for indoor wireless data transfer due to its ability to deliver high data speeds while maintaining high security and low cost in the unlicensed spectrum [1]. VLC systems are more energy-efficient since light-emitting diodes (LEDs) are simultaneously used for illumination and data transmission. Moreover, these systems have been suggested as a solution to the spectrum shortage of RF systems [2]. For low-cost implementation, VLC systems typically utilize intensity-modulation with direct-detection (IM/DD), where the information is conveyed through the intensity of the emitted light and detected by photodiodes (PDs) at the receiver. Moreover, optical orthogonal frequency-division multiplexing (OFDM) is widely used in VLC systems as a spectrally

The associate editor coordinating the review of this manuscript and approving it for publication was Barbara Masini.

efficient modulation technique, reducing inter-symbol interference (ISI). The most popular optical OFDM schemes are DC-biased optical OFDM (DCO-OFDM) and asymmetrically clipped optical OFDM (ACO-OFDM) [3], [4]; both the schemes impose Hermitian symmetry on the modulated subcarriers to guarantee a real time-domain OFDM signal. However, DCO-OFDM is more spectrally efficient compared to ACO-OFDM.

Despite the diverse advantages of VLC systems, these systems are limited by the low modulation bandwidth of LEDs which prohibits transmission at high data rates. The limited electrical bandwidth of the optical elements motivates the use of new techniques such as non-orthogonal multiple access (NOMA) [52] and spatial multiplexing in VLC systems [5], [6], [7], [8], [9]. One of the main ideas to increase the bit rate is NOMA which its key principle is to allow different users to share the same frequency resources simultaneously at the expense of multi-user interference (MUI). To perform MU detection, different users are assigned distinct power levels based on their channel gains. It is noted here that although NOMA is efficient for scenarios where the number of users is higher than the number of available orthogonal resources, its complexity grows proportionally and rapidly to the number of users. This is because the $i$th user is required to decode the messages of the $i-1$ users before detecting its signal. The spatial multiplexing simplifies the transmitter and receiver designs compared to the NOMA [52].In spatial multiplexing works, due to the unique characteristics of IM/DD, which require signals to be real and unipolar, it is very difficult to pair orthogonal users together, as in RF systems. For this reason, the NOMA technique is recently used to reduce inter-user interference (IUI) in VLC systems. However, in this paper, by considering the temporal delay between transmitter and receiver, the channel is complex in the frequency domain so that it can be proved that, similar to RF, the channels of pair users are orthogonal in a high subcarrier index when the number of LEDs is large.

Another technique that increases the data rate is spatial multiplexing which is used in two categories: single-user MIMO (SU-MIMO) and multi-user MIMO (MU-MIMO). MU-MIMO systems have several unique features distinct from SU-MIMO systems. Although both systems provide spatial multiplexing gains that effectively improve the throughput, the SU-MIMO systems are vulnerable in scenarios where the spatial multiplexing capability of a single user's channel is limited due to the signal-to-interference-plus-noise ratio (SINR) or by the number of PDs at the user side. It is well known that when the channel matrix is full rank, the capacity gain of SU-MIMO systems is scaled by $\min\{M, L\}$-fold at a high signal-to-noise ratio (SNR), where $M$ and $L$ are the number of LEDs at the access point (AP) and the number of PDs at the user side, respectively [10]. However, the major drawbacks of spatial multiplexing systems are transmitter precoding, receiver detection complexity, and inter-channel interference (ICI) caused by channel coupling. In order to solve the aforementioned drawbacks, various optical MIMO techniques have been investigated, such as spatial modulation (SM) [11], [12], [13]. Only one LED out of an array of LEDs operates at any particular time in the basic SM systems, completely eliminating the ICI. However, the drawback of SM techniques is the system performance degradation if the channel matrix is ill-conditioned.

The MU-MIMO system has been studied for VLC systems, and several precoding schemes have been proposed, which are different from conventional RF systems since only real-valued non-negative signals can be transmitted [14], [15], [16]. In [14], the performances of zero-forcing (ZF) and dirty paper coding schemes are compared for indoor VLC broadcasting systems. An optimal linear precoding transmitter is derived based on the minimum mean-squared error (MMSE) criterion in [15]. In [16], an optimal mean-squared error (MSE) precoder was designed to minimize the bit error rate (BER), under per-LED power constraints. The transceiver design was later simplified by adopting a ZF precoder. The corresponding results showed that the simplified scheme outperforms the conventional ZF precoder in terms of BER, while MSE achieves the best performance. Similar designs were proposed in [37], where an optimal ZF precoder was obtained using an iterative concave-convex procedure, aiming at maximizing the achievable per-user data rate. Then, the authors simplified the precoder design using the high SNR approximation. In [38], Shen et al. proposed a different beamforming technique aiming at maximizing the sum rate of a virtual MIMO VLC system. Beamforming was designed using the sequential parametric convex approximation method, and it has been shown through simulations that it outperforms conventional ZF-based beamforming, particularly for highly correlated VLC channels and low optical transmit power. Likewise, Marshoud et al. developed in [39] an optical adaptive precoding for downlink MIMO VLC systems, under perfect and imperfect channel state information (CSI). The corresponding BER results showed that the proposed scheme is more robust to imperfect CSI and channel correlation than conventional channel inversion precoding. In [40], the sum rate maximization problem was reformulated as a weighted MMSE (WMMSE) problem to jointly design the precoding and receive filter coefficients. A similar approach was also considered in [41]. Finally, Adasme et al. proposed in [42] a hybrid approach, called spatial TDMA (STDMA), where full connectivity is achieved by allowing simultaneous data transmission of multiple nodes within an optimized schedule. The contribution in [43] and [44] focused on precoding designs for coordinated multi-point (CoMP) MU-MIMO VLC systems. Through numerical analysis, the authors showed improvements in terms of signal-to-interference-plus-noise ratio (SINR) and weighted sum MSE (WSMSE), respectively. Additionally, Yin et al. considered in [45] and [46] different spatial division multiple access (SDMA) grouping algorithms to obtain a trade-off between the Jain's fairness index and area spectral efficiency for a CoMPVLC system through the utilization of linear ZF precoding. The authors in [47] proposed a joint precoder

and equalizer design based on interference alignment for MU multi-cell MIMO VLC systems under imperfect CSI, whereas in [48], different levels of coordination/cooperation were considered using a ZF precoder. It is worth noting that SDMA can be also realized using an angle diversity transmitter (ADT), which consists of multiple directional narrow-beam LED elements. An ADT creates independent narrow-band beams towards spatially deployed users while achieving the same coverage as a single wide beam transmitter [49]. ADTs can also replace conventional single-element transmitters in multi-cell scenarios such that more power is directed towards each user, which in turn improves the communication's reliability [50], [51].

In RF-based communication systems, one of the approaches used for increasing the achievable rate is massive MIMO (mMIMO) [19]. Some of the advantages of mMIMO technology are improving the spectral and energy efficiencies with simple linear precoding schemes, which achieve the same performance as the optimal non-linear one, thanks to using the massive number of antennas at the AP. These advantages mainly hinge on channel hardening and orthogonality of channels between the two distinct users. Therefore, the same time-frequency resource could be shared between users without causing severe IUI. In VLC, to maximize the achievable rate, using massive LEDs arrays at AP has been explored [20]. Furthermore, the paradigm of mMIMO has been explored in VLC systems recently by incorporating several LED arrays and PD arrays [22], [27]. Hence, optical OFDM can be extended to mMIMO VLC systems to further enhance the achievable rate [23] by mitigating ISI. However, indoor VLC channels are typically highly correlated since there is no phase information. The line-of-sight (LOS) scenario is mostly considered, which is unfavorable for the application of MIMO techniques and degrades the performance [18]. The authors in [24] and [25] showed that the achievable rate in mMIMO is limited due to channel correlation. Therefore, the problem of channel correlation in VLC systems is more severe due to the dominant LOS component [26]. For clarity, Table 1 summarizes the key points in the above discussion and related works.

In this paper, the MU-mMIMO-OFDM technique is proposed for indoor VLC systems where the AP is equipped with a large number of LEDs. Therefore, the AP can communicate with many users simultaneously through spatial multiplexing. This work considers the time delay between LEDs and users. Since the distances between the multiple transmitter-receiver links are different, their temporal delays are also different, which results in complex channel gain and phase differences when transformed to the frequency domain in OFDM systems. The channel vectors between the users and the AP become pairwisely orthogonal on the high index subcarrier with a massive LEDs array, considering the wideband system. Hence, the IUI can be mitigated via the simple precoding matrix that is obtained for each OFDM subcarrier. Simple linear precoding techniques such as ZF, MMSE, and maximum ratio transmission (MRT) are proposed in the frequency domain to eliminate IUI in the downlink scenario. It is worth mentioning that to the best of our knowledge; the MRT precoder is employed for the first time in MU-mMIMO-OFDM for the VLC systems. Since the VLC channel model in previous works just includes a LOS link, which is a real and positive value, the MRT precoder cannot be used. In this paper, we demonstrate that by choosing a wideband channel model for VLC and considering the temporal delay of each channel between the LEDs and users, the MRT precoder can be used to remove the IUI. Moreover, the achievable spectral efficiency and total optical power of the ZF, MMSE, and MRT precoders are obtained and compared, assuming perfect channel state information at the AP. Furthermore, the closed-form formulation for the lower bound on the average achievable sum-rate is derived.

It is worth noting that the considered channels between the LEDs and users were real and positive in the previous studies. Therefore, the system performance degraded significantly when the number of users increased. Due to the aforementioned limitations, the system throughput cannot be enhanced remarkably by simply increasing the number of LEDs. To address this limitation, we have proposed the MU-mMIMO combined with OFDM modulation, which results in complex channels among the LEDs and users in the frequency domain when the temporal delay between LEDs and users is considered in the channel model. In this case, the channels associated with different users are orthogonal when the number of LEDs approaches infinity. Moreover, it is shown that the proposed system's performance significantly outperforms the previous works by using simple linear precoders. The main contributions of this paper are summarized as follows:

- Deriving the MRT, MMSE, and ZF precoders in the MU-mMIMO-OFDM system, which eliminates the IUI effectively in the IM/DD links. It is worth noting that MMSE and ZF precoders have been used in other studies for IM/DD links. However, the achievable performance is not sufficient since the precoders have been applied to the real and positive channels. On the other hand, we derive the linear precoders for the complex channel in the frequency domain, thanks to the optical OFDM technique.
- Employing the MRT precoding for the first time in MU-mMIMO-OFDM for the VLC system, considering the wideband channel model and the temporal delay of each channel between the multiple transmitter-receiver.
- Formulating the closed-form average achievable sum-rate expressions for three linear precoding methods, including the MRT, MMSE, and ZF.
- Obtaining the proposed system's performance through Monte-Carlo simulations and analytical results. Moreover, it is demonstrated that the performance of the proposed method in this paper for all precoder techniques, i.e., ZF, MMSE, and MRT, is better than the previous work methods. Further, it is shown that the proposed method increases the achievable data rates in the VLC

**TABLE 1. Summary of the related works.**

| Refrence | System Model | Objective | Findings |
|---|---|---|---|
| [35], [36] | MU-MISO with BD precoding | Evalution of the BER | With enough transmit power, a data rate of 100 Mbps is achieved for BER=10e-6 |
| [14] | MU-MISO with ZF or ZF-DPC precoding | Maximization of the throughput and max-min fairness | ZF-DPC outperforms linear ZF, in particular when users are close to each other |
| [15] | MU-MISO with MMSE precoding | Evalution of the optimal linear MMSE precoder under perfect and imperfect CSIT | MMSE precoding achieves beast results, while proposed simplified ZF approaches MMSE performance for a small number of (or dispersed) users |
| [16] | MU-MISO with MMSE/ZF precoding | Minimization of the MSE and evaluation of the BER | MMSE precoding achieves beast results, while proposed simplified ZF approaches MMSE performance for a small nimber of (or dispersed) users |
| [37] | MU-MISO with ZF precoding | Maximization of the sum rate and max-min fairness | The generalized-inverse ZF design achieves better performance than the pseudo-inverse ZF design, in particular for high SNRs |
| [38] | MU-MISO with ZF precoding | Maximization of the sum rate | The proposed approach dose not restrict the co-channel interference to zero, and thus, achieves a higher sum rate than conventional ZF techniques |
| [39] | MU-MISO with adaptive precoding | Derivation of closed-form experssion and evalution of BER under perfect and imperfect CSIT | Adaptive precoding provides performance enhancement compared to conventional channel inversion precoding |
| [40] | MU-MISO OFDM with ZF/MMSE precoding | Evaluation of the spectral efficiency | Sub-carrier with higher index achieves a higher spectral efficiency, particularly for highly correlated users, and MMSE outperforms ZF for low transmit power and close users |
| [41] | MU-MISO with BD precoding | Maximization of the sum rate with imperfect CSIT | Robust precoding is designed using BD and WMMSE to suppress MUI and channel estimation errors |
| [42] | MU-MIMO with joint MMSE precoding and equalizing | Minimization of the MSE and evaluation of the BER in presence of CSIT errors | Proposed joint optimization method demonstrates BER improvments when experiencing imperfect CSIT |
| [43] | MU-STDMA | Minimization of the total scheduling time and power consumption | STDMA achieves full connectivity, and the proposed greedy algorithm reduces the processing time |
| [44], [45] | Multi-cell MU-MIMO CoMP with MMSE precoding | Minimization of the WSMSE | Proposed approach realizes low-complexity interference mitigation compared to CoMP JT |
| [46], [47] | CoMP SDMA with ZF precoding | Evaluation of the Jain's fairness index and of area spectral efficiency | The proposed grouping algorithm achieves better area spectral efficiency-fairness trade-off compared to existing benchmarks |
| [48] | Multi-cell MU-MIMO joint MMSE precoding and equalizing | Minimization of the MSE and sum rate evaluation with imperfect CSIT | The joint design of the precoder and equlizer efficiency reduce inter-user interference and inter-cell interference, and achieves better performance compared to existing MMSE and max-rate designs |
| [49], [50] | SDMA using ADTs | Evaluation of the throughput | The use of ADTs improves the performance of multi-user systems, and optical SDMA outperforms optical TDMA in terms of throughput |
| [51] | Attocell SDMA downlink using ADT | Derivation of closed-form expression for the spectral efficiency | inter-cell interference is mitigated and optical SDMA outperforms optical TDMA |
| [18] | MU-MIMO with AFS-based SDMA system for V-VLC | Evalution of the BER | The proposed novel SDMA approach reduces multiuser interference for V-VLC by taking advantage of modern matrix LED-based AFS. |
| [20] | m-MIMO with adaptive precoding | Evalution of the BER | Novel precoder based on SVD for ill-conditioned m-MIMO VLC channel is proposed which the precoding exponent is adaptively learned using the MSER criterion |
| [27] | MU m-MIMO with adaptive precoding | Evalution of the BER | The proposed precoding technique significantly outperforms BD based precoding in terms of BER performance |
| [23] | m-MIMO-VLC | Evalution of the SINR | The proposed system is able to work at a high data rate of 1.5 Gb/s for MU the scenario in the presence of the MU interfere |

systems and decreases the required total downlink optical power. Furthermore, our proposed system results in a higher number of users.

- Analyzing the performance of the proposed system in this paper and a previous work [27] in terms of achievable spectral efficiency and total downlink optical power. Since in [27] users are equipped with multiple PDs and in this work, they are single PD users, each user in [27] is equivalent to two single PD users in this paper. To analyze the achievable spectral efficiency, it is assumed that the total optical power in the AP is 0 dBW which is equally divided among all users. For instance, the achievable spectral efficiency improvement compared to previous work [27] is 5 bps/Hz and 3 bps/Hz for ZF/MMSE and MRT precoders, respectively, when the number of LEDs and users are 64 and 16, respectively. To analyze the required total optical power, it is assumed that the total achievable spectral

efficiency of 3.5 bits/s/Hz is equally shared among the users. Comparing the total optical power demonstrates that the ZF, MMSE, and MRT precoding improves the system performance by about 20 dBW, 30 dBW, and 44 dBW compared to previous work [27] when the number of LEDs and users are 64 and 64, respectively.

The rest of the paper is organized as follows: The system and channel models are introduced in Section II. Section III describes multiuser massive MIMO OFDM-based downlink data transmission. The precoder design is proposed in Section IV. Section V provides the downlink rate analysis. Numerical results are shown in Section VI. Finally, conclusions are presented in Section VII.

*Notation*: Throughout the paper, matrices and column vectors are in bold uppercase and bold lowercase letters, respectively. The $m$th row and $n$th column element of a matrix $\mathbf{A}$ is given by $\mathbf{A}(m, n)$. The trace of a matrix $\mathbf{A}$, denoted by $\mathrm{tr}(\mathbf{A})$. The transpose and Hermitian transpose operators for vector or matrix are expressed by $(.)^T$ and $(.)^H$. The pseudo-inverse and inverse operators for a matrix are denoted by $(.)^\dagger$ and $(.)^{-1}$, respectively. The identity matrix is expressed by $\mathbf{I}$. A real and complex normal distribution with mean $\mu$ and variance $\sigma^2$ is represented by $\mathcal{N}(\mu, \sigma^2)$ and $\mathcal{CN}(\mu, \sigma^2)$, respectively. Also, the Dirac delta function is given by $\delta(.)$. Lastly, $\mathbb{E}(.)$ expresses the expectation operation.

## II. SYSTEM AND CHANNEL MODELS

A MU-mMIMO-OFDM VLC system is depicted in Fig. 1, where a room is equipped with multiple LEDs for illumination, which can also collaborate in simultaneous data transmission to multiple users. It is assumed there is an AP with $M$-LEDs that transmits the data to $L$ single-PD users such that $L \leq M$. It is worth mentioning that single-PD users are simple, inexpensive, and power-efficient. Therefore, the multiple-LED AP serves $L$ single-PD users simultaneously using the spatial multiplexing in the same time-frequency resource.

For the VLC communications, the time-domain channel response from the $q$th LED to the $p$th user is written as

$$h^{p,q}(t) = h_{dc}^{p,q}\, \delta\left(t - t_{p,q}^{\text{delay}}\right), \tag{1}$$

where $h_{dc}^{p,q}$ and $t_{p,q}^{\text{delay}}$ are the DC channel gain of a LOS link and the temporal delay between the $q$th LED and the $p$th user, respectively. Also we have $t_{p,q}^{\text{delay}} = \frac{d_{p,q}}{c}$ where $d_{p,q}$ is the distance between the $q$th LED and the $p$th user and $c$ is the speed of light. Besides, the DC channel gain of a LOS link between the $q$th LED and the $p$th user is given by [21]

$$h_{dc}^{p,q} = \frac{\gamma_p\,(m+1)\,A_p^{\text{PD}}\cos^m\left(\phi_{p,q}\right) cos\left(\psi_{p,q}\right)}{2\pi\left(d_{p,q}\right)^2}\,\mathbb{1}_{\kappa_p}\left(\psi_{p,q}\right), \tag{2}$$

where $q \in \{1, 2, \ldots, M\}$ and $p \in \{1, 2, \ldots, L\}$, the responsivity coefficient of the PD at $p$th user is given by $\gamma_p$, and the radiance and incidence angles between $q$th LED and $p$th user are denoted by $\phi_{p,q}$ and $\psi_{p,q}$, respectively. The receiver collection area of $p$th user is $A_p^{\text{PD}}$, and the parameter $m = -\frac{\ln(2)}{\ln(\cos(\Phi_{1/2}))}$ is the order of Lambertian emission, where $\Phi_{1/2}$ is the LED semiangle at half power. Also, the indicator function $\mathbb{1}_{\kappa_p}(.)$ is defined as

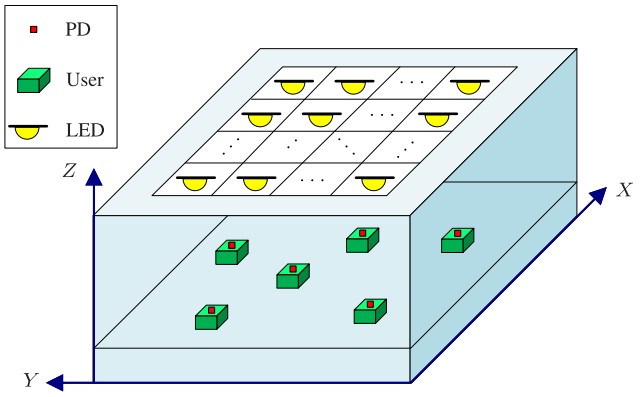


**FIGURE 1.** Indoor MU-mMIMO-OFDM VLC system.

$$\mathbb{1}_{\kappa_p}(x) = \begin{cases} 1, & \text{if } |x| \leq \kappa_p \\ 0, & \text{otherwise,} \end{cases} \tag{3}$$

where the FoV semiangle of the PD at $p$th user is denoted by $\kappa_p$.

After receiving the optical signal from each user, the PD reforms the optical signal to the electrical one. Three well-known additive and independent zero-mean Gaussian noises are called shot noise, background noise, and dark current noise added to the electrical signal. Therefore, the variance of the superimposed noises at the $p$th user is denoted by [38]

$$\sigma_p^2 = 2eP_p^{\text{opt}}B + 2e\gamma_p\chi_{\text{amb}}A_p^{\text{PD}}\left(1 - \cos\left(\kappa_p\right)\right) + i_{\text{amp}}^2\,B, \tag{4}$$

where $e$ is the electronic charge, $\chi_{\text{amb}}$ is the ambient light photocurrent, $B$ is bandwidth of the receiver, and $i_{\text{amp}}$ is the preamplifier noise current density. The parameter $P_p^{\text{opt}}$ is the average received optical power at the $p$th user. Note that the background noise is usually dominant [34], but in this work, since the bandwidth is considered wideband, the dark current noise and the background noise are dominant. Since the noises mentioned above are independent of the average received optical power, the noise variance is the same for all users, i.e., $\sigma_p^2 = \sigma^2$.

## III. MULTIUSER MASSIVE MIMO OFDM-BASED DOWNLINK DATA TRANSMISSION

The block diagram of the proposed MU-mMIMO-OFDM system is shown in Fig. 2 wherein the AP is equipped with $M$ LEDs, i.e., an array size of $M$, and serves $L$ single-PD users simultaneously. The block diagram of precoding design and IFFT are illustrated in Fig. 3. In this paper, we consider the downlink of a MU-mMIMO-OFDM.

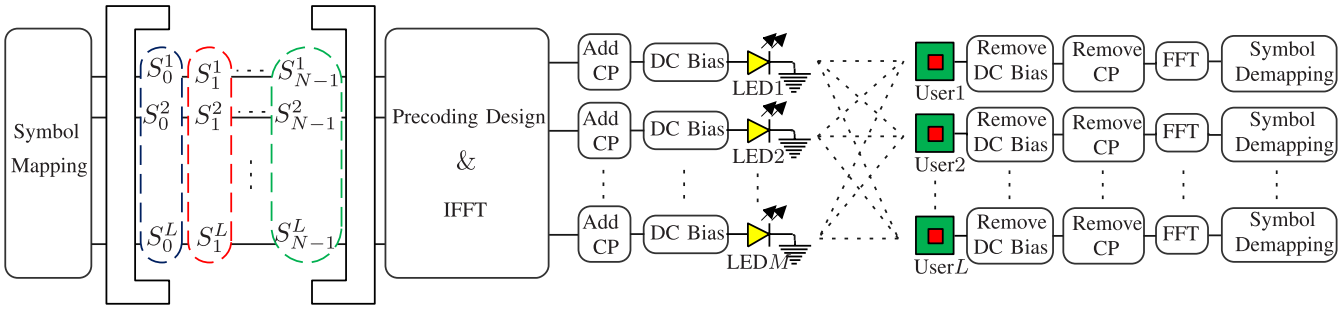


**FIGURE 2.** Block diagram of MU-mMIMO-OFDM transceiver.

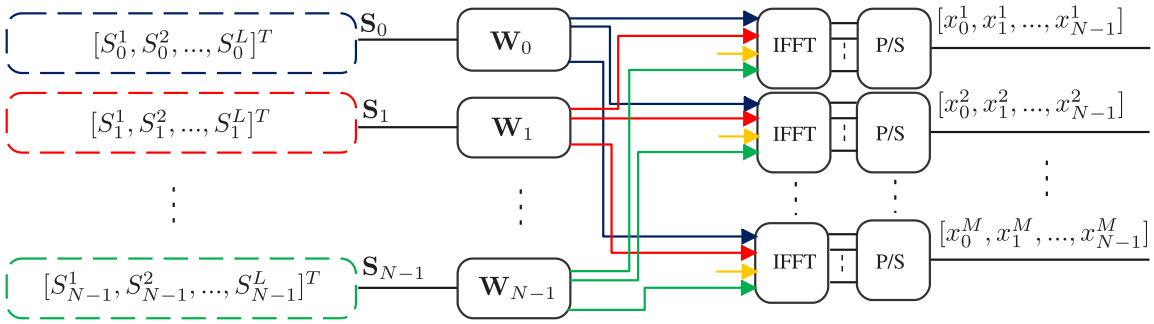


**FIGURE 3.** Block diagram of precoding design and IFFT.

As depicted in Fig. 2, the information bit stream of each user is firstly mapped onto complex-valued symbols $S_k^p$ for $k = 0, 1, \ldots, N$. That is, $S_k^p$ denotes the transmitted complex data symbol on the $k$th subcarrier for the $p$th user. Due to the use of IM/DD, to ensure that the resultant signal is real after the inverse fast Fourier transform (IFFT) operation, Hermitian symmetry should be imposed on the OFDM subcarriers, i.e., we must have $S_k^p = (S_{N-k}^p)^*$ for $k = 0, 1, \ldots, N/2 - 1$, and the subcarriers $S_0^p$ and $S_{N/2}^p$ are set to zero. Using (1), the frequency-domain channel response between the $q$th LED and the $p$th user on the $k$th subcarrier is given by

$$H_k^{p,q} = h_{dc}^{p,q} \exp\left(-\frac{j2\pi kBt_{p,q}^{delay}}{N}\right) = h_{dc}^{p,q} \exp\left(-\frac{j2\pi kBd_{p,q}}{Nc}\right). \quad (5)$$

It can be seen that the frequency domain channel response has a complex value gain, and the channel phase depends on $d_{p,q}$, $B$, and $k$. Considering the wideband system, the term $\exp\left(-\frac{j2\pi kBd_{p,q}}{Nc}\right)$ can introduce a large phase shift $\phi_{p,q} = -\frac{j2\pi kBd_{p,q}}{Nc}$ because even small values of $d_{p,q}$ are multiplied by large system bandwidth $B$, resulting in noticeable phase shifts. Since $d_{p,q}$ is random and even small values of $d_{p,q}$ can cause large phase shifts that are folded modulo $2\pi$, we can model $\phi_{p,q}$ as a random variable uniformly distributed between $-\pi$ and $\pi$. Moreover, the position of the users changes randomly with the uniform distribution in the room. Therefore, the complex channel vectors associated with the different users are spatially orthogonal to each other when the temporal delay and a large number of LEDs are considered. Hence, simple linear precoders can be proposed for complex and orthogonal channels in the frequency domain to eliminate IUI effectively. It should be noted that when the system bandwidth is not wide, the considered delay in (1) can be ignored. However, in order to achieve up to 100 Gbps high data rate transmission [17], wide bandwidth optical components are used, and the phase in the complex channel gain can not be neglected anymore. Therefore, in this paper, the bandwidth of LEDs and PDs are assumed to be wide.

In order to cancel the IUI, the AP applies a precoder on each subcarrier before generating the OFDM symbol. The precoder for the $k$th subcarrier is denoted by $W_k^{q,p}$ ($1 \le p \le L$, $1 \le q \le M$). Therefore, the superimposed precoded symbols of the $L$ users on the $k$th subcarrier and $q$th LED becomes

$$X_k^q = \sum_{p=1}^{L} W_k^{q,p} S_k^p, \qquad k = 0, 1, \ldots, N-1 \text{ and } q = 1, \ldots, M. \quad (6)$$

After performing the IFFT, the time-domain signals for the $q$th LED becomes

$$x_n^q = \frac{1}{\sqrt{N}} \sum_{k=0}^{N-1} X_k^q \exp\left(j\frac{2\pi kn}{N}\right), \quad n = 0, 1, \ldots, N-1, \quad (7)$$

which are real-valued since the Hermitian symmetry of subcarriers. $j$ is the imaginary unit, and $j = \sqrt{-1}$. Then, a cyclic prefix (CP) is added at the beginning of the time-domain OFDM symbol for each LED to combat the ISI at the receiver. Moreover, to satisfy the unipolarity restriction of IM/DD

systems, a DC bias $P_{DC}^q$ is added to $x_n^q$. Since OFDM signals have a high peak-to-average power ratio (PAPR), a DC bias can not necessarily guarantee that all the signals become non-negative and part of the signals should be clipped, leading to undesired clipping distortion. Thus, the element-wise biasing and clipping effects are given by

$$\begin{aligned} \bar{x}_n^q &= x_n^q + P_{DC}^q \\ \left(\bar{x}_n^q < 0\right) &= 0, \end{aligned} \tag{8}$$

where $P_{DC}^q$ is the DC bias for the $q$th transmitter and computed as follows [28]

$$P_{DC}^q = \mu \sqrt{\mathbb{E}\left[(x_n^q)^2\right]}, \tag{9}$$

where $\mu$ denotes the DC bias ratio. The DC bias level in decibels is defined by $10\log_{10}\left(\mu^2+1\right)$. For a larger DC bias, the signal is less clipped and results in smaller unwanted signal distortion. However, it is inefficient in terms of power since DC bias does not carry information. Therefore, there is a tradeoff between controlling the clipped distortion and wasting the power. Furthermore, a minimum DC bias ratio $\mu_0$ is defined to avoid clipping distortion [28]. When precoding is applied at the AP, the electrical power of the LEDs at the AP is different since the precoding is used at the AP side. Therefore, the DC bias is various for each LED that is calculated by

$$P_{DC}^q = \mu_0 \sqrt{\mathbb{E}\left[(x_n^q)^2\right]}. \tag{10}$$

Therefore, the optical power emitted from the $q$th LED becomes

$$\mathbb{E}\left[\bar{x}_n^q\right] = \mathbb{E}\left[x_n^q + P_{DC}^q\right] = \mathbb{E}\left[x_n^q\right] + P_{DC}^q = P_{DC}^q. \tag{11}$$

According to the central limit theorem, $x_n^q$ approximates a Gaussian distribution with zero mean when $N > 64$. Therefore, $\mathbb{E}\left[x_n^q\right] = 0$. To guarantee to have a total average power $P_{\text{total}}$ for the AP with $M$ LEDs, the transmitted signal over each LED is scaled as follows to meet the total power constraint.

$$\tilde{x}_n^q = \beta \bar{x}_n^q = \beta\left(x_n^q + P_{DC}^q\right), \tag{12}$$

where $\tilde{x}_n^q$ is the scaled transmitted signal. The scaling factor $\beta$ can be calculated as

$$\beta = \frac{P_{\text{total}}}{\mu_0 \sum_{q=1}^{M} \sqrt{\mathbb{E}\left[\left(x_n^q\right)^2\right]}}. \tag{13}$$

The transmitted optical signal experiences path loss and delay in propagating from the $q$th optical source to the $p$th receiver aperture. The optical signal is captured and translated into the electrical domain by the PD of each user. By removing the DC bias and CP and then performing the fast Fourier transform (FFT), the frequency domain symbols on the $k$th subcarrier for $p$th user are given by

$$\begin{aligned} Y_k^p &= \beta \sum_{q=1}^{M} H_k^{p,q} X_k^q + Z_k^p \\ &= \beta \sum_{q=1}^{M} \sum_{l=1}^{L} H_k^{p,q} W_k^{q,l} S_l^q + Z_k^p \\ &= \underbrace{\beta \sum_{q=1}^{M} H_k^{p,q} W_k^{q,p} S_k^p}_{\text{Desired signal}} + \underbrace{\beta \sum_{q=1}^{M} \sum_{\substack{l=1 \\ l\neq p}}^{L} H_k^{p,q} W_k^{q,l} S_l^q}_{\text{IUI}} + Z_k^p, \end{aligned} \tag{14}$$

where $Z_k^p$ denotes the equivalent noise with Gaussian distribution with zero mean and variance $\sigma^2$ on the $k$th subcarrier for $p$th user. The first term in (14) denotes the desired signal, while the second term is the IUI for the $p$th user on the $k$th subcarrier. In this case, complex channel vectors associated with different users are mutually spatially orthogonal as the number of LEDs increases. This claim is discussed in Section IV. Therefore, thanks to a large number of LEDs at the AP, IUI can be eliminated using a linear precoding technique, allowing more users to communicate in the same time-frequency resource simultaneously. We can rewrite (14) in the matrix form as

$$\mathbf{Y}_k = \beta \mathbf{H}_k \mathbf{W}_k \mathbf{S}_k + \mathbf{Z}_k, \qquad k = 0, 1, \ldots, N-1 \tag{15}$$

where $\mathbf{S}_k = \left[S_k^1, S_k^2, \ldots, S_k^L\right]^T$ and $\mathbf{Y}_k = \left[Y_k^1, Y_k^2, \ldots, Y_k^L\right]^T$ denote the transmitted and received symbol vectors on the $k$th subcarrier, $\mathbf{H_k}(p,q) = H_k^{p,q}$, $\forall p, q$ and $\mathbf{W_k}(q,p) = W_k^{q,p}$, $\forall p, q$ represent the corresponding channel and precoding matrices and $\mathbf{Z}_k = \left[Z_k^1, Z_k^2, \ldots, Z_k^L\right]^T$ is the noise vector on the $k$th subcarrier.

## IV. PRECODER DESIGN

This section presents three precoders, i.e., the MRT, ZF, and MMSE in MU-mMIMO-OFDM for the VLC system to degrade the interference term efficiently in (14).

### 1) MRT PRECODING

It is assumed that the perfect CSI, i.e., $\mathbf{H}_k$, is available at the AP. So, the linear MRT precoder matrix $\mathbf{W}_k$ of size $M \times L$ is defined as

$$\mathbf{W}_k = \xi_k \mathbf{A}_k, \tag{16}$$

where $\mathbf{A}_k$ is obtained as follows

$$\mathbf{A}_k = {\mathbf{H}_k}^H. \tag{17}$$

Moreover, $\xi_k$ is a scaling factor to satisfy the precoder gain constraint to meet the power constraint and is computed as

$$\xi_k = \frac{1}{\sqrt{\text{tr}\left({\mathbf{A}_k}^H \mathbf{A}_k\right)}}. \tag{18}$$

Therefore, the received signal of the $p$th user on the $k$th subcarrier given in (14) is reformulated as

$$Y_k^p = \beta \xi_k \left[\mathbf{H_k A_k}\right]_{p,p} S_k^p + \beta \xi_k \sum_{\substack{m=1 \\ m\neq p}}^{L} \left[\mathbf{H_k A_k}\right]_{p,m} S_k^m + Z_k^p \tag{19}$$

where $[\mathbf{H_k A_k}]_{p,p}$ and $[\mathbf{H_k A_k}]_{p,m}$ are the diagonal elements and the off-diagonal elements, respectively. Using (13) and (17), the diagonal elements can be written as

$$[\mathbf{H_k A_k}]_{p,p} = \sum_{q=1}^{M} \left(h_{dc}^{p,q}\right)^2. \tag{20}$$

Moreover, by substitution (20) into (19), we can obtain desired signal as $\beta\xi_k \sum_{q=1}^{M} \left(h_{dc}^{p,q}\right)^2$ for $p$th user on $k$th subcarrier.

As it is shown in (19), IUI depends on the off-diagonal elements. In Appendix A, we have shown that the distributions of $\frac{1}{M}[\mathbf{H_k A_k}]_{p,m}$ converge to the following Gaussian distributions,

$$\frac{1}{M}[\mathbf{H_k A_k}]_{p,m} \to \mathcal{CN}\left(\mu_0, \frac{\sigma_0^2}{M}\right). \tag{21}$$

When $M \to \infty$, we have $\mu_0 = 0$ and $\frac{\sigma_0^2}{M} \to 0$ especially for the subcarriers with larger index. Therefore, it is proved that the MRT precoder can eliminate IUI in MU-mMIMO for VLC systems when the number of LEDs in the AP increases.

#### 2) ZF PRECODER

The ZF precoding is a linear precoding technique that cancels out the inter-user interference at each user by directly forcing the interference terms to be zeros. The precoding matrix for each subcarrier can be calculated by

$$\mathbf{W_k} = \mathbf{H_k}^{\dagger}\mathrm{diag}\left(\xi_k\right) = \mathbf{H_k}^{H}\left(\mathbf{H_k}\mathbf{H_k}^{H}\right)^{-1}\mathrm{diag}\left(\xi_k\right). \tag{22}$$

The scaling factor $\xi_k$ is also calculated by (18), where $\mathbf{A_k} = \mathbf{H_k}^{H}(\mathbf{H_k}\mathbf{H_k}^{H})^{-1}$. When the channel matrix is ill-conditioned, ZF requires a large normalization factor, which will dramatically reduce the received power. Therefore, when the SNR at the receiver is low, ZF can not achieve good performance since noise instead of interference is the dominant impairment of the system [29].

#### 3) MMSE PRECODER

In linear MMSE precoding, however, the interference at the receivers is not identically zero, which achieves a tradeoff between interference and noise based on which one is the dominant part in the SINR at the receiver. The MMSE-based precoding matrix is given by [30]

$$\mathbf{W_k} = \mathbf{H_k}^{H}\left(\mathbf{H_k}\mathbf{H_k}^{H} + \mathrm{diag}\left(\sigma_{\mathbf{Z}_k}^2\right)\right)^{-1}\mathrm{diag}\left(\xi_k\right), \tag{23}$$

where $\sigma_{\mathbf{Z}_k}^2$ denotes the variance vector of $\mathbf{Z}_k$. The scaling factor $\xi_k$ can be calculated by (18), where $\mathbf{A_k} = \mathbf{H_k}^{H}\left(\mathbf{H_k}\mathbf{H_k}^{H} + \mathrm{diag}\left(\sigma_{\mathbf{Z}_k}^2\right)\right)^{-1}$.

## V. DOWNLINK RATE ANALYSIS

In wireless communication systems, the average achievable rate is a key performance metric that defines the average data rate that a wireless network can support on a given bandwidth. In what follows, we obtain the achievable data rate. Since the location of each user is random, we compute the ergodic achievable rate by expecting the instantaneous achievable rate over the random locations of the users. Therefore, we calculate the average achievable rate that AP can support. For a fixed channel realization $\mathbf{H}_k$, the noise plus MU interference term can be modeled as additive white Gaussian noise independent of $S_k^p$. Therefore, a lower bound on the achievable rate can be obtained. The average achievable sum-rate of $L$ single-PD users on the $k$th subcarrier is expressed as follows

$$R_k = L\,\mathbb{E}\left[\log_2\left(1 + \mathrm{SINR}_k^p\right)\right], \tag{24}$$

where $\mathrm{SINR}_k^p$ denotes the signal to noise plus interference ratio for the $p$th user on $k$th subcarrier, which is given as follows

$$\mathrm{SINR}_k^p = \frac{\beta^2\xi_k^2\left|[\mathbf{H_k A_k}]_{p,p}\right|^2}{\beta^2\xi_k^2\sum\limits_{\substack{l=1\\ l\neq p}}^{L}\left|[\mathbf{H_k A_k}]_{p,l}\right|^2 + \sigma^2}. \tag{25}$$

By substituting (25) into (24), the average achievable sum-rate for $L$ users on $k$th subcarrier becomes

$$R_k = L\,\mathbb{E}\left[\log_2\left(1 + \frac{\beta^2\xi_k^2\left|[\mathbf{H_k A_k}]_{p,p}\right|^2}{\beta^2\xi_k^2\sum\limits_{\substack{l=1\\ l\neq p}}^{L}\left|[\mathbf{H_k A_k}]_{p,l}\right|^2 + \sigma^2}\right)\right]. \tag{26}$$

By using the Jensen's inequality as

$$\mathbb{E}\left[\log_2\left(1 + \frac{1}{x}\right)\right] \geq \log_2\left(1 + \frac{1}{\mathbb{E}[x]}\right), \tag{27}$$

we obtain the following lower bound on the average achievable sum-rate on the $k$th subcarrier as

$$\begin{aligned} R_k &\geq \tilde{R}_k \\ &= L\,\log_2\left(1 + \mathbb{E}\left[\frac{\beta^2\xi_k^2\sum\limits_{\substack{l=1\\ l\neq p}}^{L}\left|[\mathbf{H_k A_k}]_{p,l}\right|^2 + \sigma^2}{\beta^2\xi_k^2\left|[\mathbf{H_k A_k}]_{p,p}\right|^2}\right]^{-1}\right). \end{aligned} \tag{28}$$

In the following subsections, (28) is obtained for three linear precoding methods.

### A. DOWNLINK RATE FOR MRT PRECODING

The expectation in (28) for the MRT precoder on the high subcarrier index by decomposing the fraction and using (13)

can be obtained as follows

$$\mathbb{E}\left[\frac{\beta^2\xi_k^2\sum_{\substack{l=1\\l\neq p}}^{L}\left|[\mathbf{H_k}\mathbf{A_k}]_{p,l}\right|^2+\sigma^2}{\beta^2\xi_k^2\left|[\mathbf{H_k}\mathbf{A_k}]_{p,p}\right|^2}\right] = (L-1)\,\eta_k+\frac{\sigma^2\mu_0^2}{P_{\text{total}}^2}\,\mathbb{E}\left[\frac{\text{tr}(\mathbf{A_k}\mathbf{A_k}^H)}{\left|[\mathbf{H_k}\mathbf{A_k}]_{p,p}\right|^2}\right], \quad (29)$$

where $\eta_k = \mathbb{E}\left[\frac{\left|[\mathbf{H_k}\mathbf{A_k}]_{p,l}\right|^2}{\left|[\mathbf{H_k}\mathbf{A_k}]_{p,p}\right|^2}\right]$. $\eta_k$ is the average correlation of complex channels on $k$th subcarrier. It can be proved that the expectation in (29) is simplified as $\frac{L}{M}\times\frac{1}{\mathbb{E}[(h_{dc}^{p,q})^2]}$ (see Appendix B). By rewriting (29) and substituting it into (28), the lower bound of the average achievable sum-rate of $L$ users on $k$th subcarrier for the MRT precoder becomes

$$\tilde{R}_k^{\text{MRT}} = L\,\log_2\left(1+\frac{1}{(L-1)\,\eta_k+\frac{L\mu_0^2\sigma^2}{MP_{\text{total}}^2\mathbb{E}[(h_{dc}^{p,q})^2]}}\right). \quad (30)$$

### B. DOWNLINK RATE FOR ZF PRECODING

The expectation in (28) for the ZF precoder on the high subcarrier index can be obtained as follows

$$\mathbb{E}\left[\frac{\beta^2\xi_k^2\sum_{\substack{l=1\\l\neq p}}^{L}\left|[\mathbf{H_k}\mathbf{A_k}]_{p,l}\right|^2+\sigma^2}{\beta^2\xi_k^2\left|[\mathbf{H_k}\mathbf{A_k}]_{p,p}\right|^2}\right] = \frac{\sigma^2}{\beta^2}\,\mathbb{E}[\frac{1}{\xi_k^2}], \quad (31)$$

since $\left|[\mathbf{H_k}\mathbf{A_k}]_{p,p}\right|^2 = 1$ and $\left|[\mathbf{H_k}\mathbf{A_k}]_{p,q}\right|^2 = 0$ for the ZF precoder. It can be proved that for the ZF precoder, $\mathbb{E}[\frac{1}{\xi_k^2}] = \frac{L}{M-L}\times\frac{1}{\mathbb{E}[(h_{\text{dc}}^{p,q})^2]}$ (see Appendix C). Using (13), rewriting (31), and substituting it into (28), the lower bound of the average achievable sum-rate of L users on the high subcarrier index for the ZF precoder becomes

$$\tilde{R}_k^{\text{ZF}} = L\,\log_2\left(1+\frac{(M-L)P_{\text{total}}^2\mathbb{E}\left[(h_{dc}^{p,q})^2\right]}{L\mu_0^2\sigma^2}\right). \quad (32)$$

### C. DOWNLINK RATE FOR MMSE PRECODING

The expectation in (28) for the MMSE precoder on the high subcarrier index can be obtained as (33), shown at the bottom of the page, (see Appendix D).

By substituting (33) into (28), the lower bound of the average achievable sum-rate of L users on the high subcarrier index for the MMSE precoder becomes as (34), shown at the bottom of the page.

## VI. NUMERICAL RESULTS AND DISCUSSIONS

In this section, the performance of the proposed MU-mMIMO-OFDM downlink system with MRT, ZF, and MMSE precoding over the VLC channel is analyzed in terms of achievable spectral efficiency and required total downlink optical power. Monte-Carlo simulation results are presented for different scenarios. The simulation parameters are listed in Table 2. The PD of each user is considered at the height of 0.85 $m$. Since the vertical distance between the ceiling and the receiver plane is 2.15 $m$, the horizontal distance between the LED and receiver can be as large as 2.15 $\tan(70^0) = 5.9$ $m$, which is large enough to cover the entire room. In all cases, the user can receive the optical signal from all LEDs. The LEDs are placed uniformly in a square arrangement on the ceiling with a distance of $\frac{4}{\sqrt{M}}$ from each other so that the closest LED to the wall is 0.5 $m$ away. The position of the users changes randomly with the uniform distribution in the room. We also compare the results of our work with the proposed technique in [27]. It is worth noting that the method proposed in [27] is based on users with 2 PDs whose distance is 0.1 $m$. Since in [27] users are equipped with multiple PDs and in this work, they are single PD users, each user in [27] is equivalent to two single PD users in this paper so the number of receivers in both works is equal. Throughout the figures in this section, the number of users refers to the number of users of this work, which is equivalent to twice the number of users [27].

$$\mathbb{E}\left[\frac{\beta^2\xi_k^2\sum_{\substack{l=1\\l\neq p}}^{L}\left|[\mathbf{H_k}\mathbf{A_k}]_{p,l}\right|^2+\sigma^2}{\beta^2\xi_k^2\left|[\mathbf{H_k}\mathbf{A_k}]_{p,p}\right|^2}\right] = \frac{L\mu_0^2\sigma^2}{(M-L)\,P_{\text{total}}^2\left(\mathbb{E}\left[\left(h_{dc}^{p,q}\right)^2\right]+\sigma^4\,\mathbb{E}\left[\left(h_{dc}^{p,q}\right)^{-2}\right]+2\sigma^2\right)\left(1+\sigma^2\mathbb{E}\left[\left(h_{dc}^{p,q}\right)^{-2}\right]\right)} \quad (33)$$

$$\tilde{R}_k^{\text{MMSE}} = L\,\log_2\left(1+\frac{(M-L)\,P_{\text{total}}^2\left(\mathbb{E}\left[\left(h_{dc}^{p,q}\right)^2\right]+\sigma^4\,\mathbb{E}\left[\left(h_{dc}^{p,q}\right)^{-2}\right]+2\sigma^2\right)\left(1+\sigma^2\mathbb{E}\left[\left(h_{dc}^{p,q}\right)^{-2}\right]\right)}{L\mu_0^2\sigma^2}\right) \quad (34)$$

**TABLE 2. Simulation parameters.**

| Coefficient | Symbol | Value |
|---|---|---|
| Room size (length × width × height) | $[L, W, H]$ | 5m×5m×3m |
| LED semiangle at half power | $\Phi_{1/2}$ | 70° |
| PD area | $A_{\text{PD}}$ | 1 cm$^2$ |
| PD responsivity coefficient | $\gamma_p$ | 0.4 A/W |
| Receiver half angle FOV | $\kappa_p$ | 62° |
| Preamplifier noise current density [31] | $i_{\text{amp}}$ | 5 pA/Hz$^{-1/2}$ |
| Ambient light photocurrent [32] | $\chi_{\text{amp}}$ | 10.93 A/m$^2$/Sr |
| System bandwidth [17] | $B$ | 1 GHz |
| Number of OFDM subcarriers | $N$ | 64 |
| Cyclic prefix length | $N_{\text{CP}}$ | 3 |
| Minimum DC bias factor | $\mu_0$ | 4 |

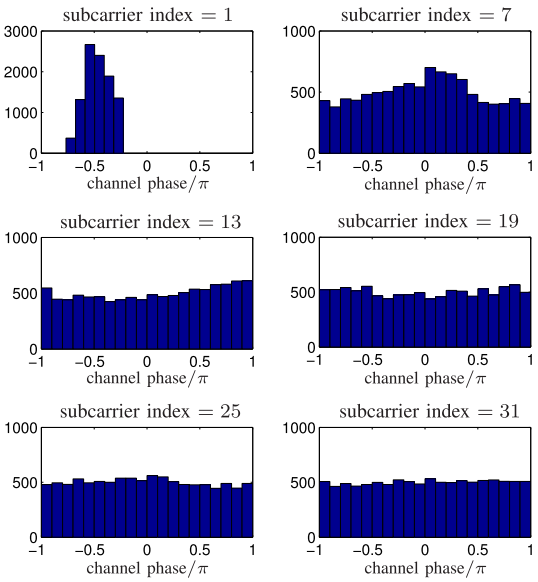


**FIGURE 4. Histogram associated with the channel phase between the LED and the user for different subcarriers.**

Fig. 4 shows the histogram of the 10,000 runs of the Monte-Carlo simulation associated with the channel phase for different OFDM subcarriers between one LED and the users whose position is changed randomly and uniformly in the room. This figure shows that the channel phase distribution is uniform between $-\pi$ and $\pi$ for the higher index OFDM subcarriers. Therefore, the IUI can be completely eliminated for the aforementioned OFDM subcarriers as the complex channel vectors associated with different users are mutually orthogonal. Since the channel phase distribution is improper for the lower index OFDM subcarriers, the proposed method cannot effectively suppress the ICI for these subcarriers.

Fig. 5 shows the average correlation of complex channels for $M = [16, 25, 64]$ LEDs in the AP as a function of OFDM subcarrier index $\eta_k$ for two different system bandwidths while keeping the number of users fixed, $L = 16$. As depicted in this

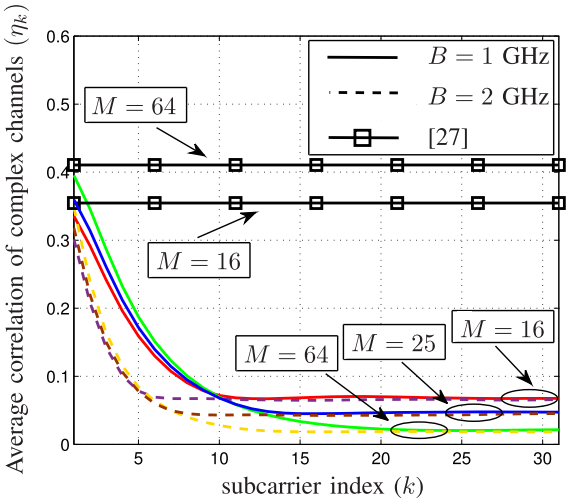


**FIGURE 5. Average of complex channels correlation on each subcarrier for different bandwidth and $L = 16$ users.**

figure, the average correlation of complex channels for the proposed method decreases as the subcarrier index increases. However, the average correlation of channels is independent of the subcarrier index for the method presented in [27]. Since our method's average correlation of complex channels is relatively low, the complex channel vectors associated with different users are mutually spatially orthogonal. Therefore, the IUI can be removed effectively using the simple linear precoders at the AP. Moreover, the correlation of complex channels decreases by increasing the number of LEDs in the proposed method while it increases in [27] due to the dominant LOS component. It can also be seen from Fig. 5 that when larger system bandwidth is selected, the number of subcarriers with less $\eta_k$ increases since the large bandwidth causes significant phase differences between complex channels on more subcarriers.

Achievable sum-rate is calculated for the $\frac{N}{2} - 1$ subcarriers that carry information by $\frac{1}{N}\sum_{k=1}^{\frac{N}{2}-1}\sum_{p=1}^{L}\log_2\left(1+\text{SINR}_k^p\right)$. To analyze the achievable spectral efficiency, it is assumed that the total optical power in the AP is 0 dBW which is equally divided among all users. Fig. 6 shows the achievable spectral efficiency versus the number of LEDs for $L = 16$ users for the MRT, ZF, and MMSE precoders. As expected, by increasing the number of LEDs, the achievable spectral efficiency also increases for all precoding techniques. When $\frac{M}{L}$ is large, achievable spectral efficiency for ZF and MMSE precoders is better than MRT precoder, while for small $\frac{M}{L}$, MRT precoder is better. This is due to the same fact that, when $\frac{M}{L} \to 1$, the complex channel matrix will be ill-condition, which causes $\xi_k$ to become large and SINR becomes low since the IUI can be effectively eliminated in our proposed method compared to [27]. For instance, the achievable spectral efficiency improvement compared to [27] is 5 bps/Hz and 3 bps/Hz for ZF/MMSE and MRT precoders, respectively, when $M = 64$.

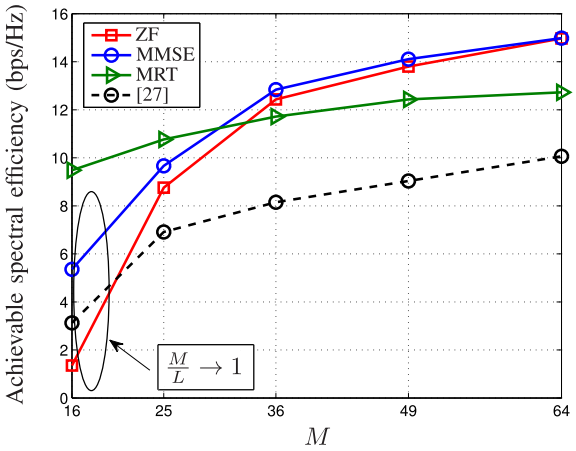


**FIGURE 6.** Achievable spectral efficiency of ZF, MMSE, and MRT precoders for different numbers of LEDs and $L = 16$ users.

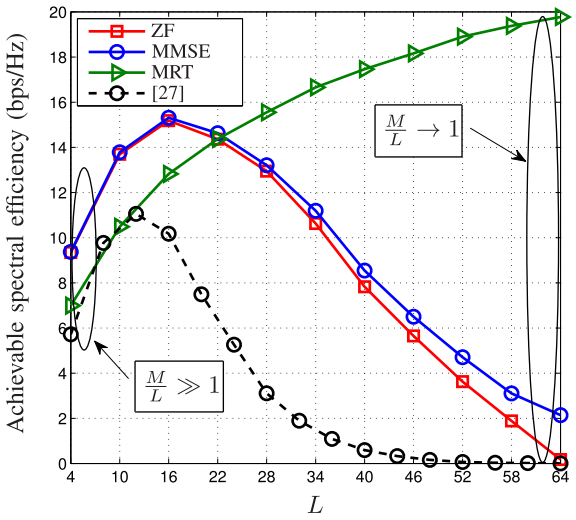


**FIGURE 7.** Achievable spectral efficiency of ZF, MMSE and MRT precoders for different number of users and $M = 64$ LEDs.

Fig. 7 depicts the achievable spectral efficiency versus the number of users for 64-LED AP for various precoders. From Fig. 7, it is observed that as $L$ increases, the achievable spectral efficiency for ZF and MMSE precoders starts to decrease, and it is a concave function of $L$, while it increases for MRT precoder. For $\frac{M}{L} \gg 1$, the performance of ZF and MMSE precoders is much better than that of the MRT precoder. For a small value of $\frac{M}{L}$, the performance of the MRT precoder is better than ZF and MMSE precoders because ZF and MMSE precoders work well at high SINR while the MRT precoder performs well at low SINR. When the number of active users becomes large, the SINR decreases since the IUI increases; hence, the performance of the ZF and MMSE precoders is degraded. The technique presented in [27] has lower performance than this paper's proposed techniques. For example, the achievable spectral efficiency improvement compared to [27] is 2 bps/Hz and 20 bps/Hz for MMSE and MRT precoders, respectively, when $L = 64$.

To analyze the required total optical power, it is assumed that the total achievable spectral efficiency of 3.5 bits/s/Hz

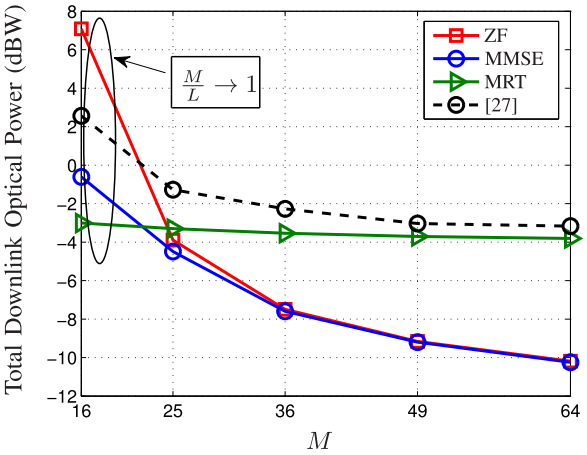


**FIGURE 8.** Total downlink optical power of ZF, MMSE, and MRT precoders for different numbers of LEDs and $L = 16$ users.

is equally shared among the users. Fig. 8 shows the required total optical power versus the number of LEDs while $L = 16$ users for the ZF, MMSE, and MRT precoders. It is observed that the required total optical power decreases as $M$ increases for all precoding techniques. However, the ZF and MMSE precoders are more power-efficient than the MRT precoder. The required total optical power of our proposed technique is better than [27]. For instance, the required total optical power in AP with 64 LEDs is $-10$ dBW using the MMSE or ZF precoders. On the other hand, the required power of the proposed method in [27] is $-3$ dBW, which is 7 dBW higher than the MMSE/ZF precoders.

Fig. 9 shows the total optical power versus the number of users for all precoders. We change $L$ from 16 to 64 while $M = 64$. It is observed from Fig. 9 that as the $L$ increases, the total downlink optical power of ZF and MMSE precoders keeps on increasing rapidly while the downlink power of the MRT precoder decreases slowly. With the increase of $L$, the total downlink optical power of ZF and MMSE precoders is quite large as compared to the MRT precoder. This is due to the same fact that ZF and MMSE precoders work well at high SINR while the MRT precoder performs well at low SINR. When $L$ is large, the value of SINR is low, and the performance of the MRT precoder is better than other techniques. It can be seen that the required total downlink optical power in [27] is higher than the techniques proposed in this paper. Comparing the total optical power demonstrates that the ZF, MMSE, and MRT precoding improves the system performance by about 20 dBW, 30 dBW, and 44 dBW compared to [27] when $L = 64$.

Fig. 10 demonstrates the average achievable sum-rate of the proposed system with ZF, MMSE, and MRT precoders for a different number of users for both Monte-Carlo simulations and numerical results. We assume 64 LEDs for the AP, and the average achievable sum-rate of the $31^{\text{th}}$ subcarrier has been shown. As clearly seen from Fig. 10, our exact closed-from expressions provide an identical match to the Monte-Carlo simulation results. Since $M$ has been considered

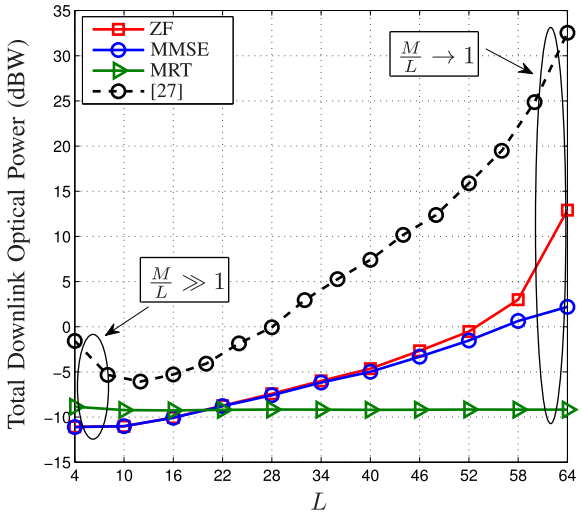


**FIGURE 9.** Total downlink optical power of ZF, MMSE, and MRT precoders for different numbers of users and $M = 64$ LEDs.

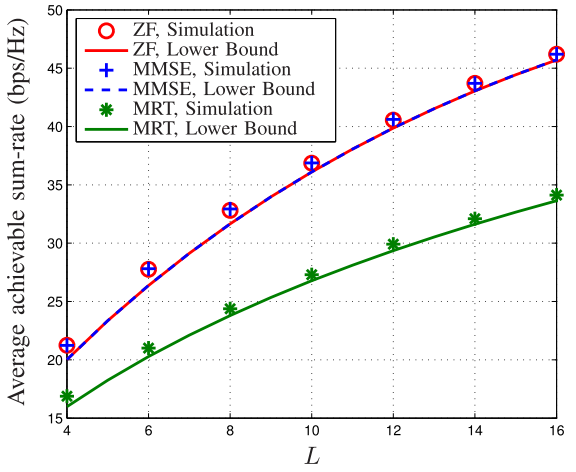


**FIGURE 10.** Average achievable sum-rate of ZF, MMSE and MRT precoders for different number of users and $M = 64$ LEDs on $k = 31^{\text{th}}$ subcarrier.

large Jensen's inequality is close to equality. Thus the lower bound of average sum rates is close to simulation results. Furthermore, the average achievable sum-rate increases as the number of users increase because the IUI is efficiently eliminated in the proposed method.

## VII. CONCLUSION

In this paper, MU-mMIMO-OFDM is studied for VLC systems, considering the phase differences of channel matrices in the frequency domain induced by the distance differences of the multiple transmitter-receiver links. The ZF, MMSE, and MRT precoding techniques are obtained for the proposed method on the complex channel matrices for each subcarrier, which is less correlated when the phase differences are considered. Also, when the number of LEDs in the AP is considered large, the complex channel correlation between different users will be negligible, resulting in effectively removing the IUI. The simulation results show that the performance of ZF and MMSE is better when the number of LEDs in AP is much larger than users. In this case, ZF and MMSE will achieve a higher data rate and will be more power-efficient as compared to MRT. However, when the ratio of the number of LEDs in AP to users is not large, the performance of MRT is superior to ZF. Moreover, the proposed method for the employed ZF, MMSE, and MRT outperforms the previously proposed methods. For instance, the total optical power for the ZF, MMSE, and MRT precoding improves the system performance by about 20 dBW, 30 dBW, and 44 dBW compared to previously proposed methods when the number of LEDs in AP and users are 64 and 64, respectively. Moreover, closed-form expressions for the lower bound on the average achievable sum-rate for all precoding techniques are derived. An excellent match between analytical results and simulations verified the accuracy of our derived expressions for the average achievable sum-rate.

## APPENDIX A

The off-diagonal elements can be written as

$$[\mathbf{H_k A_k}]_{p,m} = \sum_{q=1}^{M} \left(h_{dc}^{p,q}\right)^2 \exp\left(-\frac{j2\pi kB\left(d_{p,q} - d_{m,q}\right)}{Nc}\right). \tag{35}$$

When $M \to \infty$, according to the central limit theorem, the distributions of $\frac{1}{M}[\mathbf{H_k A_k}]_{p,m}$ converge to Gaussian distributions as follows

$$\frac{1}{M}[\mathbf{H_k A_k}]_{p,m} \to \mathcal{CN}\left(\mu_0, \frac{\sigma_0^2}{M}\right), \tag{36}$$

where,

$$\mu_0 = \mathbb{E}\left[\left(h_{dc}^{p,q}\right)^2 \exp\left(-\frac{j2\pi kBd_{p,q}}{Nc}\right)\right]\mathbb{E}\left[\exp\left(\frac{j2\pi kBd_{m,q}}{Nc}\right)\right]. \tag{37}$$

It can be seen that phase of $\exp\left(\frac{j2\pi kBd_{m,q}}{Nc}\right)$ depends on $d_{m,q}$. Considering the different temporal delay between the $q$th transmitter and $m$th user, the phase of $\exp\left(\frac{j2\pi kBd_{m,q}}{Nc}\right)$ has the uniform distribution between $-\pi$ and $\pi$ on high subcarriers, if the $M$ are selected large. Therefore, on high subcarriers $\mathbb{E}\left[\exp\left(\frac{j2\pi kBd_{m,q}}{Nc}\right)\right] = 0$, $\mu_0 = 0$. As $M \to \infty$, $\frac{\sigma_0^2}{M} \to 0$, variances of distribution approach zero.

## APPENDIX B

In (29), the expectation can be simplified by substituting $\mathbf{A}_k$ as follows

$$\mathbb{E}\left[\frac{\mathrm{tr}(\mathbf{A_k A_k}^H)}{\left|[\mathbf{H_k A_k}]_{p,p}\right|^2}\right] = \mathbb{E}\left[\frac{\sum_{j=1}^{L}\sum_{q=1}^{M}\left(h_{dc}^{j,q}\right)^2}{\left(\sum_{i=1}^{M}\left(h_{dc}^{p,i}\right)^2\right)^2}\right] \tag{38a}$$

$$= \mathbb{E}\left[\sum_{j=1}^{L}\left(\frac{\sum_{q=1}^{M}\left(h_{dc}^{j,q}\right)^2}{\left(\sum_{i=1}^{M}\left(h_{dc}^{p,i}\right)^2\right)^2}\right)\right] \tag{38b}$$

$$= L\,\mathbb{E}\left[\frac{1}{\sum_{i=1}^{M}\left(h_{dc}^{p,i}\right)^2}\right] \tag{38c}$$

$$\geq \frac{L}{M}\times\frac{1}{\mathbb{E}\left[\left(h_{dc}^{p,q}\right)^2\right]}. \tag{38d}$$

By use of the Jensen's inequality, (38d) is obtained.

## APPENDIX C

By substituting (18) into $\mathbb{E}\left[\frac{1}{\xi_k^2}\right]$, it becomes

$$\mathbb{E}\left[\frac{1}{\xi_k^2}\right] = \mathbb{E}\left[\mathrm{tr}\left(\mathbf{A_k}^H\mathbf{A_k}\right)\right] \tag{39a}$$

$$= \mathbb{E}\left[\mathrm{tr}\left(\left(\mathbf{H_k}\mathbf{H_k}^H\right)^{-1}\mathbf{H_k}\mathbf{H_k}^H\left(\mathbf{H_k}\mathbf{H_k}^H\right)^{-1}\right)\right] \tag{39b}$$

$$= \mathbb{E}\left[\mathrm{tr}\left(\mathbf{H_k}\mathbf{H_k}^H\right)^{-1}\right] \tag{39c}$$

$$= \mathrm{tr}\left(\mathbb{E}\left[\left(\mathbf{H_k}\mathbf{H_k}^H\right)^{-1}\right]\right). \tag{39d}$$

By substituting $\mathbf{A_k}$ in (39a) for ZF precoder, (39b) is obtained. Since $\left(\mathbf{H_k}\mathbf{H_k}^H\right)^{-1}\mathbf{H_k}\mathbf{H_k}^H = \mathbf{I}$, (39b) is summarized as (39c). Using the linearity property of expectation and trace operators, (39d) is obtained from (39c). As shown from (20) and (21), matrix $\mathbf{H_k}\mathbf{H_k}^H$ on high subcarrier index is diagonal when $M$ is large. $\frac{1}{\mathrm{tr}\left(\mathbb{E}\left[\left(\mathbf{H_k}\mathbf{H_k}^H\right)^{-1}\right]\right)}$ is the diversity order. The diversity order measures the number of independent paths over which the data is received [33]. Diversity order of ZF precoding is $\frac{M}{L}-1$ when $\mathbb{E}\left[\left(h_{dc}^{p,q}\right)^2\right]=1$. Therefore, $\mathbb{E}\left[\frac{1}{\xi_k^2}\right]$ is obtained as follows

$$\mathbb{E}\left[\frac{1}{\xi_k^2}\right] = \frac{L}{M-L}\times\frac{1}{\mathbb{E}\left[(h_{dc}^{p,q})^2\right]}. \tag{40}$$

## APPENDIX D

For the MMSE precoder, matrix $\mathbb{E}[\mathbf{H_k}\mathbf{A_k}]$ can be expressed

$$\mathbb{E}\left[\mathbf{H_k}\mathbf{A_k}\right] = \mathbb{E}\left[\mathbf{H_k}\mathbf{H_k}^H\left(\mathbf{H_k}\mathbf{H_k}^H + \mathrm{diag}\left(\sigma_{\mathbf{Z}_k}^2\right)\right)^{-1}\right] \tag{41a}$$

$$= \mathbb{E}\left[\mathbf{H_k}\mathbf{H_k}^H\left(\mathbf{H_k}\mathbf{H_k}^H + \sigma^2\mathbf{I}\right)^{-1}\right]. \tag{41b}$$

Assuming that the noise variance in all users is equal to $\sigma^2$, (41a) is rewritten as (41b). As shown from (20) and (21), matrix $\mathbf{H_k}\mathbf{H_k}^H$ on high subcarrier index is diagonal when $M$ is large. Therefore, $\mathbb{E}\left[\mathbf{H_k}\mathbf{A_k}\right]_{p,p} = \mathbb{E}\left[\frac{(h_{dc}^{p,q})^2}{(h_{dc}^{p,q})^2+\sigma^2}\right]$ and $\mathbb{E}\left[\mathbf{H_k}\mathbf{A_k}\right]_{p,l} = 0$. By using of the Jensen's inequality, $\frac{1}{1+\sigma^2\mathbb{E}\left[\frac{1}{(h_{dc}^{p,q})^2}\right]}$ is a lower bound of $\mathbb{E}\left[\frac{(h_{dc}^{p,q})^2}{(h_{dc}^{p,q})^2+\sigma^2}\right]$. Hence, the expectation in (28) for the MMSE precoder on the high subcarrier index can be simplified as follows

$$\mathbb{E}\left[\frac{\beta^2\xi_k^2\sum_{\substack{l=1\\ l\neq p}}^{L}\left|\left[\mathbf{H_k}\mathbf{A_k}\right]_{p,l}\right|^2+\sigma^2}{\beta^2\xi_k^2\left|\left[\mathbf{H_k}\mathbf{A_k}\right]_{p,p}\right|^2}\right] = \frac{\sigma^2\mu_0^2}{P_{\text{total}}^2}\,\frac{1}{1+\sigma^2\mathbb{E}\left[(h_{dc}^{p,q})^{-2}\right]}\,\mathbb{E}\left[\frac{1}{\xi_k^2}\right]. \tag{42}$$

By substituting (18) into $\mathbb{E}\left[\frac{1}{\xi_k^2}\right]$, it becomes

$$\mathbb{E}\left[\frac{1}{\xi_k^2}\right] = \mathbb{E}\left[\mathrm{tr}\left(\mathbf{A_k}^H\mathbf{A_k}\right)\right]$$

$$= \mathbb{E}\left[\mathrm{tr}\left(\left(\mathbf{H_k}\mathbf{H_k}^H + \mathrm{diag}(\sigma_{Z_k}^2)\right)^{-1}\mathbf{H_k}\mathbf{H_k}^H\left(\mathbf{H_k}\mathbf{H_k}^H + \mathrm{diag}\left(\sigma_{Z_k}^2\right)\right)^{-1}\right)\right]$$

$$= \mathbb{E}[\mathrm{tr}\left(\left(\mathbf{H_k}\mathbf{H_k}^H + \sigma^2 I\right)^{-1}\mathbf{H_k}\mathbf{H_k}^H\left(\mathbf{H_k}\mathbf{H_k}^H + \sigma^2\mathbf{I}\right)^{-1}\right)] \tag{43a}$$

$$= \mathrm{tr}\left(\mathbb{E}\left[\left(\mathbf{H_k}\mathbf{H_k}^H + \sigma^2\mathbf{I}\right)^{-1}\mathbf{H_k}\mathbf{H_k}^H\left(\mathbf{H_k}\mathbf{H_k}^H + \sigma^2\mathbf{I}\right)^{-1}\right]\right). \tag{43b}$$

By substituting $\mathbf{A_k}$ in (43a) for MMSE precoder, (43b) is obtained. Assuming that the noise variance in all users is equal to $\sigma^2$, (43b) is rewritten as (40c). Due to the linearity of expectation and trace operators, (43d) is obtained from (43c). Due to the diagonality of the $\mathbf{H_k}\mathbf{H_k}^H$ matrix on the high subcarrier index when $M$ is large, $\mathbb{E}\left[\frac{1}{\xi_k^2}\right]$ is obtained as follows

$$\mathbb{E}\left[\frac{1}{\xi_k^2}\right] = \frac{L}{M-L}\times\mathbb{E}\left[\frac{(h_{dc}^{p,q})^2}{\left((h_{dc}^{p,q})^2+\sigma^2\right)^2}\right]. \tag{44}$$

The expectation in (44) is simplified as follows

$$\mathbb{E}\left[\frac{(h_{dc}^{p,q})^2}{((h_{dc}^{p,q})^2+\sigma^2)^2}\right] = \mathbb{E}\left[\frac{1}{(h_{dc}^{p,q}+\frac{\sigma^2}{h_{dc}^{p,q}})^2}\right] \tag{45a}$$

$$= \mathbb{E}\left[\frac{1}{(h_{dc}^{p,q})^2 + 2\sigma^2 + \frac{\sigma^4}{(h_{dc}^{p,q})^2}}\right] \quad (45b)$$

$$\geq \frac{1}{\mathbb{E}\left[(h_{dc}^{p,q})^2 + 2\sigma^2 + \frac{\sigma^4}{(h_{dc}^{p,q})^2}\right]} \quad (45c)$$

$$= \frac{1}{\mathbb{E}\left[(h_{dc}^{p,q})^2\right] + \sigma^4\,\mathbb{E}[(h_{dc}^{p,q})^{-2}] + 2\sigma^2}. \quad (45d)$$

By using of the Jensen's inequality, (45c) is obtained. Therefore, $\mathbb{E}\left[\frac{1}{\xi_k^2}\right]$ is expressed as follows

$$\mathbb{E}\left[\frac{1}{\xi_k^2}\right] = \frac{L}{M-L} \times \frac{1}{\mathbb{E}\left[(h_{dc}^{p,q})^2\right] + \sigma^4\,\mathbb{E}\left[(h_{dc}^{p,q})^{-2}\right] + 2\sigma^2}. \quad (46)$$

Hence, by substituting (46) into (42), (33) is obtained.

## ACKNOWLEDGMENT

The authors would like to express their deep gratitude to Dr. Mohammad Javad Emadi for his patient guidance, enthusiasm, and valuable critiques of this research work.

## REFERENCES

[1] L. E. M. Matheus, A. B. Vieira, L. F. Vieira, M. A. Vieira, and O. Gnawali, "Visible light communication: Concepts, applications and challenges," *IEEE Commun. Surveys Tuts.*, vol. 21, no. 4, pp. 3204–3237, 4th Quart., 2019.

[2] S. Rehman, S. Ullah, P. Chong, S. Yongchareon, and D. Komosny, "Visible light communication: A system perspective—Overview and challenges," *Sensors*, vol. 19, no. 5, p. 1153, Mar. 2019.

[3] P. P. Jativa, C. A. Azurdia-Meza, M. R. Canizares, D. Zabala-Blanco, and I. Soto, "BER performance of OFDM-based visible light communication systems," in *Proc. IEEE CHILEAN Conf. Electr., Electron. Eng., Inf. Commun. Technol. (CHILECON)*, Nov. 2019, pp. 1–6.

[4] X. Deng, S. Mardanikorani, G. Zhou, and J.-P. M. G. Linnartz, "DC-bias for optical OFDM in visible light communications," *IEEE Access*, vol. 7, pp. 98319–98330, 2019.

[5] C.-W. Hsu, C.-W. Chow, I.-C. Lu, Y.-L. Liu, C.-H. Yeh, and Y. Liu, "High speed imaging 3 × 3 MIMO phosphor white-light LED based visible light communication system," *IEEE Photon. J.*, vol. 8, no. 6, pp. 1–6, Dec. 2016.

[6] S. Li, B. Huang, and Z. Xu, "Experimental MIMO VLC systems using tricolor LED transmitters and receivers," in *Proc. IEEE Globecom Workshops (GC Wkshps)*, Dec. 2017, pp. 1–6.

[7] C. Chen, Y. Yang, X. Deng, P. Du, and H. Yang, "Space division multiple access with distributed user grouping for multi-user MIMO-VLC systems," *IEEE Open J. Commun. Soc.*, vol. 1, pp. 943–956, 2020.

[8] J. Lian, Y. Gao, P. Wu, G. Zhu, and Y. Wang, "Indoor MIMO VLC systems using optical orthogonal frequency division multiple access," *Opt. Commun.*, vol. 485, Apr. 2021, Art. no. 126728.

[9] S. A. Nezamalhosseini and L. R. Chen, "Optimal power allocation for MIMO underwater wireless optical communication systems using channel state information at the transmitter," *IEEE J. Ocean. Eng.*, vol. 46, no. 1, pp. 319–325, Jan. 2021.

[10] D. Tse and P. Viswanath, *Fundamentals of Wireless Communication*. Cambridge, U.K.: Cambridge Univ. Press, 2005.

[11] N.-T. Nguyen, Q.-T. Nguyen, and N.-H. Nguyen, "The index-based optical spatial modulation scheme in optical MIMO," in *Proc. Int. Conf. Adv. Technol. Commun. (ATC)*, Oct. 2016, pp. 191–196.

[12] C. He, T. Q. Wang, and J. Armstrong, "Performance comparison between spatial multiplexing and spatial modulation in indoor MIMO visible light communication systems," in *Proc. IEEE Int. Conf. Commun. (ICC)*, May 2016, pp. 1–6.

[13] J.-Y. Wang, J.-X. Zhu, S.-H. Lin, and J.-B. Wang, "Adaptive spatial modulation based visible light communications: SER analysis and optimization," *IEEE Photon. J.*, vol. 10, no. 3, pp. 1–14, Jun. 2018.

[14] Z. Yu, R. J. Baxley, and G. T. Zhou, "Multi-user MISO broadcasting for indoor visible light communication," in *Proc. IEEE Int. Conf. Acoust., Speech Signal Process.*, May 2013, pp. 4849–4853.

[15] H. Ma, L. Lampe, and S. Hranilovic, "Robust MMSE linear precoding for visible light communication broadcasting systems," in *Proc. IEEE Globecom Workshops (GC Wkshps)*, Dec. 2013, pp. 1081–1086.

[16] B. Li, J. Wang, R. Zhang, H. Shen, C. Zhao, and L. Hanzo, "Multiuser MISO transceiver design for indoor downlink visible light communication under per-LED optical power constraints," *IEEE Photon. J.*, vol. 7, no. 4, pp. 1–15, Aug. 2015.

[17] D. Tsonev, S. Videv, and H. Haas, "Towards a 100 Gb/s visible light wireless access network," *Opt. Exp.*, vol. 23, no. 2, pp. 1627–1637, Jan. 2015.

[18] C. Tebruegge, A. Memedi, and F. Dressler, "Reduced multiuser-interference for vehicular VLC using SDMA and matrix headlights," in *Proc. IEEE Global Commun. Conf. (GLOBECOM)*, Dec. 2019, pp. 1–6.

[19] E. G. Larsson, O. Edfors, F. Tufvesson, and T. L. Marzetta, "Massive MIMO for next generation wireless systems," *IEEE Commun. Mag.*, vol. 52, no. 2, pp. 186–195, Feb. 2014.

[20] S. Jain, R. Mitra, and V. Bhatia, "Adaptive precoding-based detection algorithm for massive MIMO visible light communication," *IEEE Commun. Lett.*, vol. 22, no. 9, pp. 1842–1845, Sep. 2018.

[21] J. M. Kahn and J. R. Barry, "Wireless infrared communications," *Proc. IEEE*, vol. 85, no. 2, pp. 265–298, Feb. 1997.

[22] R. Chataut and R. Akl, "Massive MIMO systems for 5G and beyond networks-overview, recent trends, challenges, and future research direction," *Sensors*, vol. 20, no. 10, pp. 27–53, 2020.

[23] S. H. Younus, A. A. Al-Hameed, M. Alhartomi, and A. T. Hussein, "Massive MIMO for indoor VLC systems," in *Proc. 22nd Int. Conf. Transparent Opt. Netw. (ICTON)*, Jul. 2020, pp. 1–6.

[24] S. Biswas, C. Masouros, and T. Ratnarajah, "Performance analysis of large multiuser MIMO systems with space-constrained 2-D antenna arrays," *IEEE Trans. Wireless Commun.*, vol. 15, no. 5, pp. 3492–3505, May 2016.

[25] J. Joung, E. Kurniawan, and S. Sun, "Channel correlation modeling and its application to massive MIMO channel feedback reduction," *IEEE Trans. Veh. Technol.*, vol. 66, no. 5, pp. 3787–3797, 2017.

[26] D. Karunatilaka, F. Zafar, V. Kalavally, and R. Parthiban, "LED based indoor visible light communications: State of the art," *IEEE Commun. Surveys Tuts.*, vol. 17, no. 3, pp. 1649–1678, 3rd Quart., 2015.

[27] R. Mitra and V. Bhatia, "Precoding technique for ill-conditioned massive MIMO-VLC system," in *Proc. IEEE 87th Veh. Technol. Conf. (VTC Spring)*, Jun. 2018, pp. 1–5.

[28] S. D. Dissanayake and J. Armstrong, "Comparison of ACO-OFDM, DCO-OFDM and ADO-OFDM in IM/DD systems," *J. Lightw. Technol.*, vol. 31, no. 7, pp. 1063–1072, Apr. 1, 2013.

[29] Q. H. Spencer, A. L. Swindlehurst, and M. Haardt, "Zero-forcing methods for downlink spatial multiplexing in multiuser MIMO channels," *IEEE Trans. Signal Process.*, vol. 52, no. 2, pp. 461–471, Feb. 2004.

[30] Q. H. Spencer, C. B. Peel, A. L. Swindlehurst, and M. Haardt, "An introduction to the multiuser MIMO downlink," *IEEE Commun. Mag.*, vol. 42, no. 10, pp. 60–67, Oct. 2004.

[31] D. C. O'Brien and M. Katz, "Optical wireless communications within fourth-generation wireless systems [invited]," *J. Opt. Netw.*, vol. 4, no. 6, p. 312, 2005.

[32] A. J. C. Moreira, R. T. Valadas, and A. M. de Oliveira Duarte, "Optical interference produced by artificial light," *Wireless Netw.*, vol. 3, no. 2, pp. 131–140, 1997.

[33] A. H. Mehana and A. Nosratinia, "Diversity of MIMO linear precoding," *IEEE Trans. Inf. Theory*, vol. 60, no. 2, pp. 1019–1038, Feb. 2014.

[34] S. Zargari, M. Kolivand, S. A. Nezamalhosseini, B. Abolhassani, L. R. Chen, and M. H. Kahaei, "Resource allocation of hybrid VLC/RF systems with light energy harvesting," *IEEE Trans. Green Commun. Netw.*, vol. 6, no. 1, pp. 600–612, Mar. 2022.

[35] J. Chen, Y. Hong, Z. Wang, and C. Yu, "Precoded visible light communications," in *Proc. 9th Int. Conf. Inf., Commun. Signal Process.*, Dec. 2013, pp. 1–4.

[36] Y. Hong, J. Chen, Z. Wang, and C. Yu, "Performance of a precoding MIMO system for decentralized multiuser indoor visible light communications," *IEEE Photon. J.*, vol. 5, no. 4, Aug. 2013, Art. no. 7800211.

[37] T. V. Pham, H. Le-Minh, and A. T. Pham, "Multi-user visible light communication broadcast channels with zero-forcing precoding," *IEEE Trans. Commun.*, vol. 65, no. 6, pp. 2509–2521, Jun. 2017.

[38] H. Shen, Y. Deng, W. Xu, and C. Zhao, "Rate maximization for downlink multiuser visible light communications," *IEEE Access*, vol. 4, pp. 6567–6573, 2017.
[39] H. Marshoud, P. C. Sofotasios, S. Muhaidat, B. S. Sharif, and G. K. Karagiannidis, "Optical adaptive precoding for visible light communications," *IEEE Access*, vol. 6, pp. 22121–22130, 2018.
[40] Z. Zeng and H. Du, "Robust precoding scheme for multi-user MIMO visible light communication system," in *Proc. 25th Eur. Signal Process. Conf. (EUSIPCO)*, Aug. 2017, pp. 2546–2550.
[41] K. Ying, H. Qian, R. J. Baxley, and S. Yao, "Joint optimization of precoder and equalizer in MIMO VLC systems," *IEEE J. Sel. Areas Commun.*, vol. 33, no. 9, pp. 1949–1958, Sep. 2015.
[42] P. Adasme, F. Seguel, I. Soto, and E. S. Juan, "Spatial time division multiple access for visible light communication networks," in *Proc. 1st South Amer. Colloq. Visible Light Commun. (SACVLC)*, Nov. 2017, pp. 1–6.
[43] H. Ma, L. Lampe, and S. Hranilovic, "Coordinated broadcasting for multiuser indoor visible light communication systems," *IEEE Trans. Commun.*, vol. 63, no. 9, pp. 3313–3324, Sep. 2015.
[44] H. Ma, A. Mostafa, L. Lampe, and S. Hranilovic, "Coordinated beamforming for downlink visible light communication networks," *IEEE Trans. Commun.*, vol. 66, no. 8, pp. 3571–3582, Aug. 2018.
[45] L. Yin, X. Wu, and H. Haas, "SDMA grouping in coordinated multipoint VLC systems," in *Proc. IEEE Summer Topicals Meeting Ser. (SUM)*, Jul. 2015, pp. 169–170.
[46] L. Yin, X. Wu, H. Haas, and L. Hanzo, "Low-complexity SDMA user-grouping for the CoMP-VLC downlink," in *Proc. IEEE Global Commun. Conf. (GLOBECOM)*, Dec. 2015, pp. 1–6.
[47] H. Yang, C. Chen, W.-D. Zhong, and A. Alphones, "Joint precoder and equalizer design for multi-user multi-cell MIMO VLC systems," *IEEE Trans. Veh. Technol.*, vol. 67, no. 12, pp. 11354–11364, Oct. 2018.
[48] T. V. Pham and A. T. Pham, "Coordination/cooperation strategies and optimal zero-forcing precoding design for multi-user multi-cell VLC networks," *IEEE Trans. Commun.*, vol. 67, no. 6, pp. 4240–4251, Jun. 2019.
[49] Z. Chen and H. Haas, "Space division multiple access in visible light communications," in *Proc. IEEE Int. Conf. Commun. (ICC)*, Jun. 2015, pp. 5115–5119.
[50] Z. Chen, D. A. Basnayaka, and H. Haas, "Space division multiple access for optical attocell network using angle diversity transmitters," *J. Lightw. Technol.*, vol. 35, no. 11, pp. 2118–2131, Jun. 1, 2017.
[51] H. Sifaou, A. Kammoun, K.-H. Park, and M.-S. Alouini, "Robust transceivers design for multi-stream multi-user MIMO visible light communication," *IEEE Access*, vol. 5, pp. 26387–26399, 2017.
[52] H. Sadat, M. Abaza, A. Mansour, and A. Alfalou, "A survey of NOMA for VLC systems: Research challenges and future trends," *Sensors*, vol. 22, no. 4, p. 1395, Feb. 2022.

**MOHAMMAD JAVAD ZAKAVI** was born in Nur, Iran, in 1997. He received the B.Sc. and M.Sc. degrees (Hons.) in communication engineering from the Iran University of Science and Technology (IUST), Tehran, Iran, in 2019 and 2021, respectively. He is currently pursuing the Ph.D. degree in communication engineering with the Sharif University of Technology (SUT), Tehran. His research interests include visible light communications, wireless communications, massive MIMO, and IRS-assisted communication.

**S. ALIREZA NEZAMALHOSSEINI** received the B.Sc. degree in electrical engineering from the Amirkabir University of Technology, Tehran, Iran, in 2006, and the M.Sc. and Ph.D. degrees in electrical engineering from the Sharif University of Technology (SUT), Tehran, in 2008 and 2013, respectively. In September 2018, he joined the Department of Electrical Engineering, Iran University of Science and Technology (IUST), where he is currently an Assistant Professor. His current research interests include optical wireless communications, with particular emphasis on visible light communications and underwater wireless optical communications, signal processing for wireless communications, with particular emphasis on multicarrier and massive MIMO systems, and multimode optical fiber communications.

**LAWRENCE R. CHEN** (Senior Member, IEEE) received the B.Eng. degree in electrical engineering and mathematics from McGill University, Montreal, QC, Canada, in 1995, and the M.A.Sc. and Ph.D. degrees in electrical and computer engineering from the University of Toronto, Toronto, ON, Canada, in 1997 and 2000, respectively. Since 2000, he has been with the Department of Electrical and Computer Engineering, McGill University. His research interests include optical communications, silicon photonics, microwave photonics, and engineering education (particularly learning systems and learning mechanisms). He is a fellow of Optica. He was the Guest Co-Editor of the IEEE/OSA JOURNAL OF LIGHTWAVE TECHNOLOGY Special Issue on Microwave Photonics published, in 2020, the Principal Guest Editor of the IEEE JOURNAL OF SELECTED TOPICS IN QUANTUM ELECTRONICS Special Issue on Optical Signal Processing published, in 2021, and the Principal Guest Editor of the IEEE JOURNAL OF SELECTED TOPICS IN QUANTUM ELECTRONICS Special Issue on Photonic Signal Processing to be published, in 2023.